RESEARCH ARTICLE

National Science Open
2: 20220033, 2023
https://doi.org/10.1360/nso/20220033

Materials Science

Unconventional ferroelectricity in half-filling states of antiparallel stacking of twisted WSe_2

Liheng An[1,2,#], Zishu Zhou[1,2,#], Xuemeng Feng[1,2,#], Meizhen Huang[1,2], Xiangbin Cai[1,2], Yong Chen[1,2], Pei Zhao[3], Xi Dai[1], Jingdi Zhang[1], Wang Yao[3], Junwei Liu[1,*] & Ning Wang[1,2,*]

[1]*Department of Physics and Center for Quantum Materials, the Hong Kong University of Science and Technology, Hong Kong, China;*
[2]*William Mong Institute of Nano Science and Technology, the Hong Kong University of Science and Technology, Hong Kong, China;*
[3]*Department of Physics, University of Hong Kong, Hong Kong, China*

#Contributed equally to this work.
*Corresponding authors (emails: phwang@ust.hk (Ning Wang); liuj@ust.hk (Junwei Liu))

Received 31 May 2022; Revised 7 September 2022; Accepted 12 September 2022; Published online 3 January 2023

Abstract: We report on emergence of an abnormal electronic polarization in twisted double bilayer WSe_2 in antiparallel interface stacking geometry, where local centrosymmetry of atomic registries at the twist interface does not favor the spontaneous electronic polarizations as recently observed in the parallel interface stacking geometry. The unconventional ferroelectric behaviors probed by electronic transport measurement occur at half filling insulating states at 1.5 K and gradually disappear at about 40 K. Single band Hubbard model based on the triangular moiré lattice and the interlayer charge transfer controlled by insulating phase transition are proposed to interpret the formation of electronic polarization states near half filling in twisted WSe_2 devices. Our work highlights the prominent role of many-body electronic interaction in fostering novel quantum states in moiré-structured systems.

Keywords: two-dimensional semiconductor, twist moiré, ferroelectricity, electron interaction, electronic transport

INTRODUCTION

Stacking layered materials with small twist angles or with small lattice mismatches produce moiré superlattices that realize modulation of potentials at much larger spatial scale resulting in remarkable electronic properties [1,2], such as correlated insulators [3], superconductivity states [4], and ferromagnetism [5,6]. More recently, a new type of ferroelectricity has been created and identified through the stacking of layered van der Waals heterostructures of hexagonal boron nitride (BN) and semiconducting transition metal dichalcogenides (TMDCs) [7–13], of which the bulk structures forbid ferroelectricity. Ferroelectricity in twisted TMDCs is created by the structurally relaxed parallel stacking geometry and the moiré interface formed by the parallel stacking is also called 'R-stacking'. Two types of locally R-stacking domains coexist in one moiré unit cell, featuring opposite spontaneous polarizations of the same magnitude. The macroscopic ferroelectric polarization results from the dynamic bending of domain walls that microscopically favors polarization in one direction over the other [14].

According to the definition in previous publications [14–16], two identical 1H-WSe_2 layers stacked to each

other at zero twisting angle will result in the parallel stacking interface. The antiparallel stacking interface is formed by rotating one of these two identical 1H-WSe_2 layers at 60° and stacking the two layers together. Opposite to parallel stacking geometry, in antiparallel stacking WSe_2, the electronic polarization locked to the local atomic registries is expected to be vanishingly small when local centrosymmetric geometry is fully respected [17]. Therefore, to date, neither theoretical nor experimental study has reported on the emergence of ferroelectricity in antiparallel stacked configuration. As we previously identified that strong electron-electron correlation effects occurred in twisted WSe_2 [15,16,18], it is anticipated that the correlation-driven insulating states in the moiré bands of antiparallel stacking WSe_2 may modulate interlayer charge transfer and even induce electronic polarization. It has been well acknowledged that the polarization in crystalline structures can be divided into ionic polarization and electronic state polarization [19]. In contrast to conventional displacive (ions or molecules) ferroelectricity, electronic polarization (the difference in polarization between two different states in the same structure) is rare in materials and normally occurs in a strongly correlated electronic system [20,21].

In this study, we choose double bilayer WSe_2 to construct antiparallel stacking moiré superlattices and field-effect devices, of which the moiré flat bands with Γ pocket holes contribute to the electrical transport. Stacking two identical bilayer WSe_2 with a twist angle near 0° results in the so-called antiparallel interface (Figure 1). In each moiré unit cell, there are three important high-symmetry stacking sites as labeled by AB, $B^{W/W}$ and $B^{Se/Se}$ separated by boundary regions (BR). AB sites are the energetically favorable regions (near 2H registry), whereas other regions correspond to higher energy states. The high symmetry sites periodically modulate the electronic states in real space and therefore produce moiré bands [22].

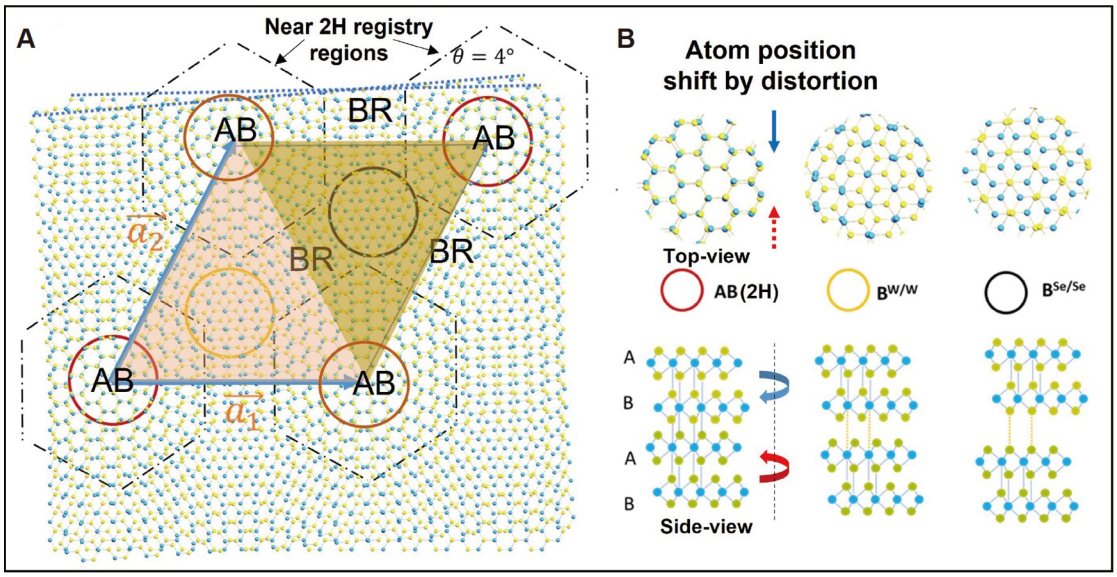

Figure 1 (A) Moiré superlattice structure constructed by antiparallel stacking of twisted double bilayer WSe_2. The circles denote the high symmetry stacking sites. The hexagons (dashed lines) indicate the near 2H registry regions. BR indicates the boundary regions. (B) The atomic configurations of the high symmetry stacking sites of AB, $B^{W/W}$ and $B^{Se/Se}$ and their side views of these sites. Blue and red arrows denote the atom positions shifts from top and bottom layers of WSe_2.

RESULTS AND DISCUSSION

Atomically thin WSe_2 is mechanically exfoliated from high-quality bulk crystals of WSe_2. Field-effect devices are fabricated based on twisted double bilayer WSe_2 by using the tear-and-stack method [15,18,23]. To achieve a large size of uniform moiré lattices, we select a relatively large twist angle of about 4°. Atomically thin BN layers are used to form an encapsulated device structure. The electrical connection to the twisted WSe_2 channel is realized by Pt electrodes (with a matched work function to WSe_2) which offer a good efficiency for current injection. The device performance has been effectively improved by this kind of electrode design. The measured channel resistance is about 5 kΩ at a modest carrier density of 3×10^{12} cm^{-2} and the field-effect carrier mobility approaches 2000 cm^2 V^{-1} s^{-1}. The device channel size is limited to 1×10 μm to achieve a good uniformity of the twist angle. The strong interlayer coupling between WSe_2 bilayers results in the rise of the Γ valley band top (about 80 meV higher than that of the K valley) [18]. Details of device fabrication and measurement principles are presented in the Supplementary Information.

Our density functional calculation, in the absence of many-body Coulomb interaction, confirms the dependence of spontaneous electrical polarization on stacking registry, as found in the parallel stacking interface [14], but denies its existence in the antiparallel stacking interface of twisted double bilayer WSe_2 of arbitrary lattice match (Figure S2). Atomic-resolution electron microscopic imaging reveals several noteworthy features in our samples (Figure 2A and 2C). We first verify the twist angle and moiré periodicity by electron diffraction (Figure 2B). The general moiré structural features well match the model shown in

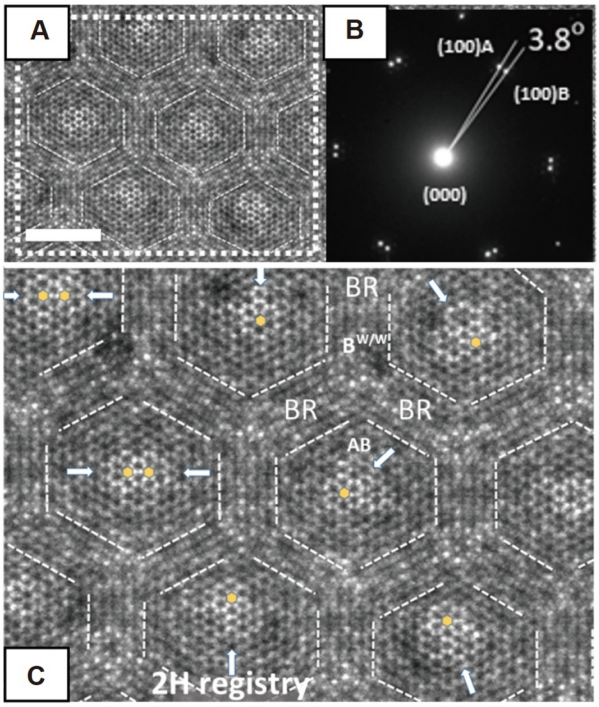

Figure 2 (A) Transmission electron microscopy (TEM) image of the antiparallel twisted double bilayer WSe_2. (B) Electron diffraction pattern taken from the area in (A). The twist angle is determined to be about 3.8°. (C) An enlarged image of the region marked by the white dashed rectangle in (A). The positions of exact 2H stacking are marked by yellow hexagons (dashed lines). The white thick arrows indicate the directions of the 2H registry shifts. The scale bar is 3 nm.

Figure 1A. However, we find that the AB regions (marked by hexagons) are expandable and the location of exact AB stacking (marked by the hexagonal dots and white arrows) is switchable. More analyses can be found in Figure S3. These structural instability features deviate from the theoretical model, and therefore hint on the necessity to incorporate new mechanisms for insights into the origin of the moiré band modulation near half filling under different electrical fields as discussed in more detail later.

The electronic states of the antiparallel stacking bilayer WSe_2 channel in the field-effect device shown in Figure 3 are tuned by the top (V_{TG}) and bottom (V_{BG}) electrical gates. V_{TG} and V_{BG} can together linearly tune the carrier density ($n = (C_{BG}V_{BG} + C_{TG}V_{TG})/e$) and displacement field ($D = (C_{BG}V_{BG} - C_{TG}V_{TG})/2\varepsilon_0$) of this p-type semiconductor electronic system, where C and V represent device capacitances and gate voltages, e is the elementary charge and ε_0 is the vacuum permittivity. A negative V_{TG} (−12 to −14 V) is first applied in order to achieve good electrical contacts to the twisted WSe_2 and injection of holes in the device channel. Forward scanning of V_{BG} (from −60 to +60 V) is to release holes from the channel and increase D. At V_{BG} = +60 V, the hole density in the channel is very low. The typical electrical transport characteristics of the p-type antiparallel twisted WSe_2 devices measured by a four-probe configuration at 1.5 K are shown in Figure 3, in which a quick decrease of the resistance (R_{xx}) by decreasing V_{BG} from +60 V indicates that the Fermi level touches the edge of the topmost moiré band. By further decreasing V_{BG}, two metallic and two insulating states are detected. The metallic and insulating states are verified by measuring their R_{xx} at different temperatures as demonstrated in Figure 4A. We further verify that the two insulating states are from the correlation-induced

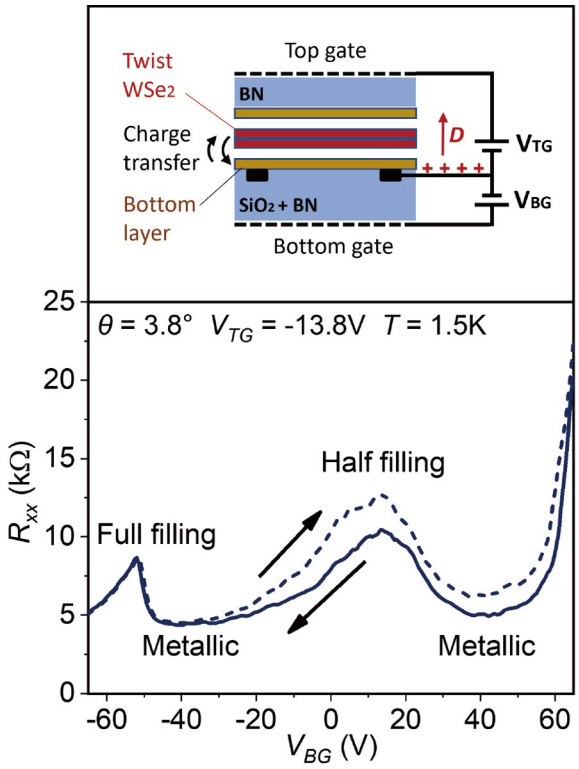

Figure 3 The structure of the field-effect device built based on antiparallel stacking of twisted double bilayer WSe_2 and the typical resistance hysteresis measured in the device. The device is double gated by the top and bottom gates in order to tune the carrier concentration and the displacement field (D). By fixing the top gate (V_{TG}) at −13.8 V, scanning the bottom gate (V_{BG}) results in the change of the filling states. Forward-backward scans (indicated by the dashed/solid lines) of V_{BG} show a clear resistance hysteresis.

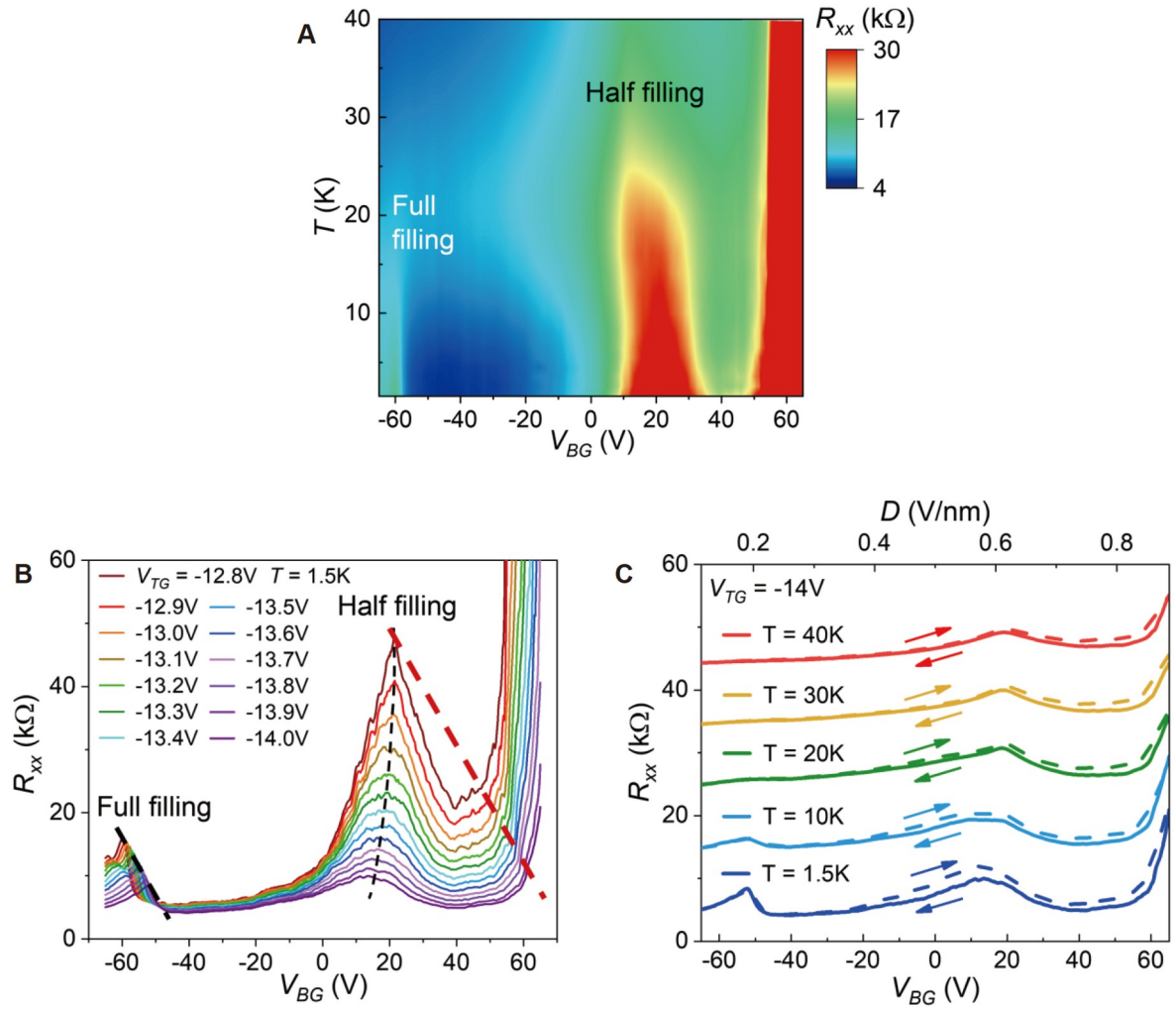

Figure 4 (A) Phase diagram plotted based on transport measurement. The half filling states gradually disappear when temperature is higher than 40 K. (B) Displacement field effects (by setting V_{TG} at different voltages and scanning V_{BG}) on the full filling and half filling states. The full and half filling states behave differently by changing the displacement fields. The black/red thick dashed lines indicate the ideal full/half filling peak positions. The black thin dashed line indicates the peak positions of half filling states measured. (C) Temperature dependence of the resistance hysteresis. The hysteresis loops gradually disappear at about 40 K.

splitting of the topmost moiré band [2,23,24], corresponding to the half and full filling states respectively. The full filling gap is resolved at a carrier density of $n = 9.8 \times 10^{12}$ cm^{-2} with two holes per unit cell to fully occupy the first moiré band [25]. The resistance peak emerging near $n = 5 \times 10^{12}$–6×10^{12} cm^{-2} represents the important half filling insulating states driven by strong correlation effects. By forward-and-backward scanning V_{BG} for several times, an obvious resistance hysteresis is repeatedly observed around half filling states (Figure 3). At half filling, when V_{TG} is set at −13.8 V, the forward scanning (−60 to +60 V) leads to a high resistance state of about 12.5 kΩ, while the backward scanning yields a low resistance state of about 10 kΩ. Such a resistance difference can be considered as the appearance of internal electric fields [13] from charge polarization (perpendicular to the moiré lattice plane) states in the system. We have carried out each measurement for five times to ensure the reproducibility of the hysteresis loops. In addition, measurements of

the *I-V* curves at the half filling states also confirm that the forward and backward scanning of gate voltages result in different channel resistances (Figure S9). To rule out the possibility that the BN dielectric layers or metal lead interfaces in the devices could potentially generate a similar hysteretic resistivity, we fabricated and measured reference devices for comparison. We also performed different gate scanning rates during hysteretic resistivity measurements and did not observe any impurity/charge trapping effect. All these additional experiments evidence that BN or charge trapping effects do not play a role in the observed hysteretic resistivity near half filling states in our samples (see details in the Supplementary Information).

The appearance of the electrical polarization characteristics in the antiparallel stacking interface structures of WSe_2 is abnormal. Different from conventional [19] and newly discovered layered van der Waals ferroelectricity [7–13,26–30], the electrical polarization in our samples is highly relevant to correlation effects which are temperature dependent. As shown in Figure 4A, the half filling insulating states gradually disappear when temperature is higher than about 40 K. The largest hysteresis we observed at 1.5 K also gradually disappears when temperature approaches to about 40 K (Figure 4C). All these phenomena are very different from that of the ferroelectricity observed in the parallel stacking geometry of TMDCs where the spontaneous electronic polarization survives at room temperature, not relevant to filling states at all, further differentiating the origins of the ferroelectricity effects between the two twist moiré systems.

Here, we try to elucidate the abnormal electrical polarization characteristics based on the following facts. The transport data are from the contribution of the Γ valley edge of WSe_2 valance bands [18] and the ultra-flat moiré bands (survived up to 4° twist angles [31]) are spatially associated with the AB sites in the antiparallel stacking interface of WSe_2 [16]. AB sites form a triangular lattice which can be considered as a mimic triangular lattice of the Hubbard model (Figure 5A). The topmost moiré band is separated from the rest and its charge distribution is tightly localized at the moiré potential minima of AB sites. Double occupancy of AB sites is suppressed due to the strong on-site Coulomb repulsion potential U, resulting in moiré band splitting to lower (LHB) and upper (UHB) Hubbard bands [32].

Ideally, the carrier densities at full/half filling of the Hubbard bands are purely determined by the moiré periodicity and obtained by $n_0=4 / (\sqrt{3}\lambda^2)$, where λ is the moiré superlattice constant. We first focus on the R_{xx} peak positions of full filling states as a reference to test the functionality of the two gates. By setting V_{TG} and scanning V_{BG} (Figure 4B), we confirm that the injected density n (hole carriers in p-type WSe_2) at full filling (the gap position) as characterized by R_{xx} peaks are all correctly tuned by the two gates. This is reflected by the change of the full filling peak positions as outlined by the inclined straight dashed line in Figure 4B. By increasing V_{TG}, the full filling peak positions shift to right side, meaning that along this dashed line, the carrier density is unchanged. Because both full and half filling densities are fixed by the moiré lattice geometry [33], the R_{xx} peaks at half filling should also follow a straight line parallel to the full filling peak line. However, the peak positions at half filling obviously shift to left side (towards higher hole concentration regions). This suggests that when increasing the D field, more holes are needed to be injected into the system in order to completely fill the LHB as displayed more clearly in Figure 5C. In addition, we noticed that the R_{xx} at half filling decreases by increasing D, which could be interpreted as that the Hubbard gap U becomes narrow accordingly. These interesting experimental data suggest two following possible physical pictures: (1) D enhances new electronic states involved in the half filling states in the moiré system; or (2) increasing D could narrow the Hubbard band gap U.

We now provide a theoretical picture to intuitively interpret the correlation-effect-induced electronic polarization based on the interlayer charge transfer controlled by electric fields and insulating phase transition. For a large *D* field applied to the double bilayer twisted device, it is possible that the entire low-energy moiré bands become layer polarized, as reported in the unconventional electronic polarization in bilayer graphene heterostructures [9]. Similarly, electrons occupying a moiré band at low energy could locate on a specific WSe_2 layer in the device. It is also reasonable to assume that LHB/UHB locates at the interface between the two inner WSe_2 layers (Figure 3). In our device design, the electrodes directly connect to the bottom WSe_2 layer and holes are firstly filled preferably in the bottom layer. We then propose that the observed *D*-dependent shift of the half filling peak is due to the involvement of new electronic states. Figure 5B schematically shows the additional band (B) coexisted with the Hubbard bands which contributes to the new electronic states. This band can be considered as the contribution from the bottom WSe_2 layer directly connected to the electrodes for hole injection. The inner two layers which host LHB/UHB states are actually not directly connected by the electrodes.

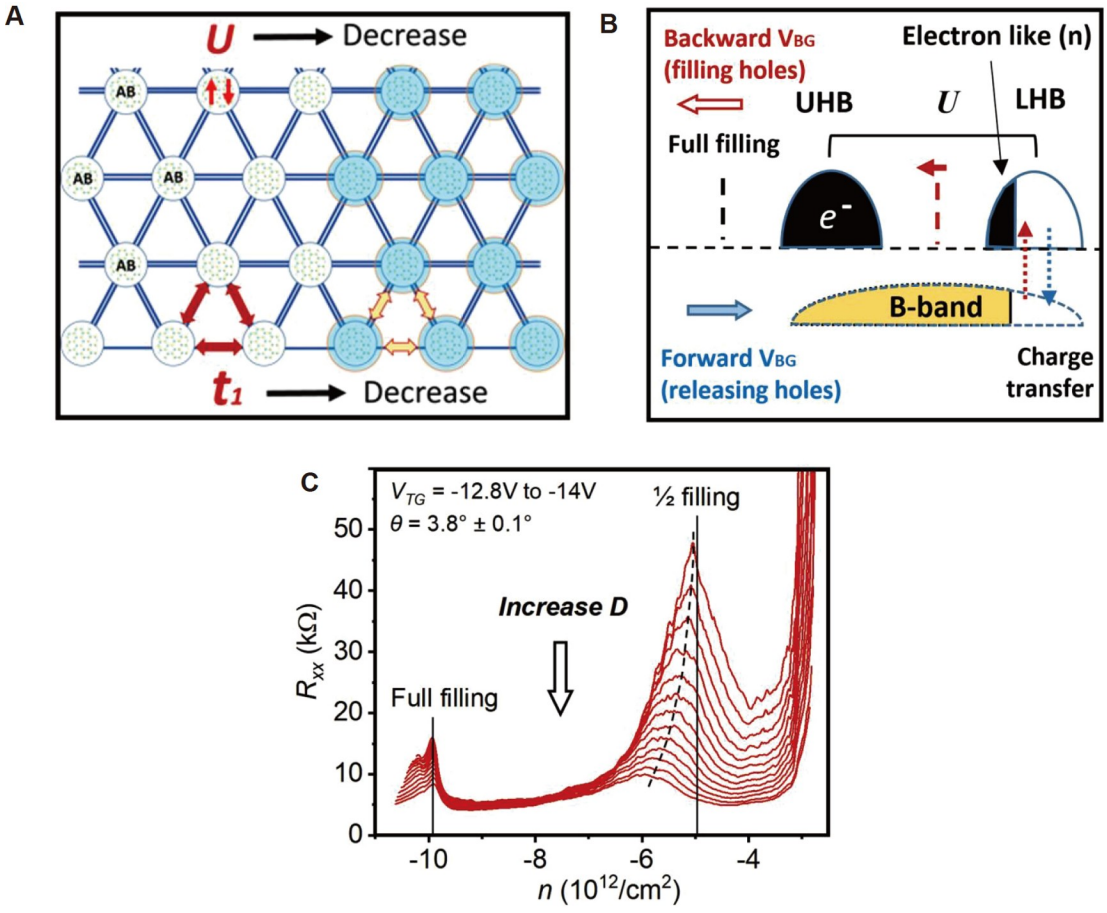

Figure 5 (A) A mimic triangular lattice of the Hubbard model for the AB sites and the variation of *U* and *t* due to AB site expansion. (B) Carrier transfer between the B-band and LHB/UHB. Forward scanning of V_{BG} results in the releasing of holes and the backward scanning of V_{BG} results in the filling of holes in the bands. Charge transferring between the B-band and LHB/UHB shows different behaviors near the gap region of the Hubbard bands. (C) Displacement field effects on the full filling and half filling gap positions. The full filling states are independent of the *D* field as indicated by the thin solid line. However, the half filling is *D*-dependent which deviates from the ideal positions as indicated by the right side thin solid line.

At a fixed D field, the backward scanning of V_{BG} (starting from +60 V) means filling holes into the electron-occupied LHB first (Figure 5B). In our p-type WSe_2 moiré system, the charge carriers which contribute to the transport measurement are holes in the valance band. Before adding holes into the valance band, all states are occupied by electrons. We use solid color (black and yellow) to illustrate the electron occupied states in the LHB and UHB in Figure 5B. By tuning the Fermi level, holes are firstly injected into the LHB and then into the UHB. Because of the involvement of the B-band, the apparent Hubbard gap position may shift to left side. During backward V_{BG} scanning, hole carriers transfer from the B-band to LHB. This interlayer charge transfer is driven by the potential associated with the gates and D field [34]. The bottom WSe_2 layer offers the B-band which is p-type under the same gating condition (larger than the threshold gate voltage). Figure 5B shows the band alignment and the carrier transfer direction between the bands. The hole filling process allows current to flow easily from B-band (p-type) to the Hubbard bands (p-type) across the spatial layer interface (similar to a p-p isotype junction [35]). Near half filling, however, the states at the bottom edge of LHB are electron-like (n-type). Holes transfer across a p-n anisotype junction (the forward biasing of a p-n junction) is less resistive. Therefore, filling LHB/UHB driven by backward V_{BG} scanning is less resistive. For the forward V_{BG} scanning, however, holes are released from LHB/UHB to the B-band. Near half filling, the p-n anisotype characteristic at the interface severely restricts holes reversely flowing through the anisotype junction (analogous to the reverse biasing of a p-n junction). The consequence is that more holes are retained in the moiré layer when the forward scanning is near half filling, while the holes in the B-layer are always released to the electrodes normally during V_{BG} scanning. Therefore, the charge polarization between the moiré layer and the B-layer is established. The extra holes in the moiré layer countervail only a part of D field strength (Figure S11B), resulting in a higher R_{xx} compared with that in the opposite direction of backward scanning V_{BG}. This is because R_{xx} is inversely proportional to the strength of the D field as revealed experimentally in Figure 5C. This mechanism supports the transport data of the R_{xx} hysteresis in Figure 3. We now conclude that the two electrical polarization states are the result of more versus less occupation of the Hubbard bands driven by the interlayer carrier transfer modulated by the insulating phase transition during D field scanning near half filling states. This abnormal electronic polarization effect has been repeatedly observed in the devices with twist angles ranging from 3.8°–4.2° (see more data in the Supplementary Information).

Electronic ferroelectricity caused by electron correlation has been proposed and studied previously based on Hubbard models in different bulk material systems [20,21], in which parameters of Coulomb repulsion potential U and hopping energy t are critical. In our moiré system, the expandable AB sites driven by correlation effects or D fields [26,27] could modulate U and t. This is because the local AB sites (near 2H registry) in our samples are expandable (also deviating from an ideal local 2H registry) involving the atomic rearrangement of the boundaries to surrounding regions. Therefore, the expanded local 2H registry together with the boundaries surrounding these regions do not hold the centrosymmetric geometry according to our electron microscopy results (see more details in the Supplementary Information). The expansion of AB sites (increasing the energy favorable area) driven by the D field could provide the driving force for decreasing U, since increasing AB site area can effectively lower U to host two electrons with opposite spins in one AB site. At present, it is still not clear whether the deviation of the half filling R_{xx} peak under different D fields is solely due to the interplay between the Hubbard bands and B-band or partially due to the D field modulation (e.g., D-field-induced electronic state instability) of the electronic states in the Hubbard bands. To this end,

further experimental and theoretical investigations are needed. Our discovery of the abnormal ferroelectricity behaviors suggests a new platform for further exploring the flat band properties tunable by an electric field, particularly the correlation-induced insulating states at the half filling states adjacent to the superconductivity states in this two-dimensional moiré system.

Data availability

The original data are available from corresponding authors upon reasonable request. Details of device fabrication, measurement principles and proposed mechanisms are presented in Supplementary Information.

Acknowledgements

We are grateful to the technical support from Dr. Yuan Cai from the Materials Characterization and Preparation Facility at the Hong Kong University of Science and Technology.

Funding

This work was supported by the National Key R&D Program of China (2020YFA 0309600), the Hong Kong Research Grants Council (AoE/P-701/20, C6025-19G, 16305919 ECS26302118, 16303720, 16305019, 16306220 and N_HKUST626/18), the National Natural Science Foundation of China (NSFC20SC07), and the William Mong Institute of Nano Science and Technology.

Author contributions

N.W. initiated and supervised the project. L.A. designed the research, device structure, measurement and data analysis. L.A., Z.Z., and X.F. fabricated the device and collected the data. L.A. and N.W. wrote the manuscript. M.H., J.Z., X.D. and J.L. contributed to the data analysis. P.Z. and W.Y. contributed to calculation. X.C. and Y.C. contributed to the sample preparation.

Conflict of interest

The authors declare that they have no conflict of interest.

Supplementary information

The supporting information is available online at https://doi.org/10.1360/nso/20220033. The supporting materials are published as submitted, without typesetting or editing. The responsibility for scientific accuracy and content remains entirely with the authors.

References

1 Kennes DM, Claassen M, Xian L, *et al.* Moiré heterostructures as a condensed-matter quantum simulator. *Nat Phys* 2021; **17**: 155–163.

2 Bistritzer R, MacDonald AH. Moiré bands in twisted double-layer graphene. *Proc Natl Acad Sci USA* 2011; **108**: 12233–12237.

3 Cao Y, Fatemi V, Demir A, *et al.* Correlated insulator behaviour at half-filling in magic-angle graphene superlattices. *Nature* 2018; **556**: 80–84.

4 Cao Y, Fatemi V, Fang S, *et al.* Unconventional superconductivity in magic-angle graphene superlattices. *Nature* 2018; **556**: 43–50.

5 Sharpe AL, Fox EJ, Barnard AW, *et al.* Emergent ferromagnetism near three-quarters filling in twisted bilayer graphene. *Science* 2019; **365**: 605–608.

6 Serlin M, Tschirhart CL, Polshyn H, *et al.* Intrinsic quantized anomalous Hall effect in a moiré heterostructure. *Science* 2020; **367**: 900–903.

7 Vizner Stern M, Waschitz Y, Cao W, *et al.* Interfacial ferroelectricity by van der Waals sliding. *Science* 2021; **372**: 1462–1466.

8 Yasuda K, Wang X, Watanabe K, *et al.* Stacking-engineered ferroelectricity in bilayer boron nitride. *Science* 2021; **372**: 1458–1462.

9 Zheng Z, Ma Q, Bi Z, *et al.* Unconventional ferroelectricity in moiré heterostructures. *Nature* 2020; **588**: 71–76.

10 Woods CR, Ares P, Nevison-Andrews H, *et al.* Charge-polarized interfacial superlattices in marginally twisted hexagonal boron nitride. *Nat Commun* 2021; **12**: 347.

11 Li L, Wu M. Binary compound bilayer and multilayer with vertical polarizations: Two-dimensional ferroelectrics, multiferroics, and nanogenerators. *ACS Nano* 2017; **11**: 6382–6388.

12 Wang X, Yasuda K, Zhang Y, *et al*. Interfacial ferroelectricity in rhombohedral-stacked bilayer transition metal dichalcogenides. *Nat Nanotechnol* 2022; **17**: 367–371.

13 Weston A, Castanon EG, Enaldiev V, *et al*. Interfacial ferroelectricity in marginally twisted 2D semiconductors. *Nat Nanotechnol* 2022; **17**: 390–395.

14 Zhao P, Xiao C, Yao W. Universal superlattice potential for 2D materials from twisted interface inside h-BN substrate. *npj 2D Mater Appl* 2021; **5**: 38.

15 Cai X, An L, Feng X, *et al.* Layer-dependent interface reconstruction and strain modulation in twisted WSe_2. *Nanoscale* 2021; **13**: 13624–13630.

16 Li E, Hu JX, Feng X, *et al.* Lattice reconstruction induced multiple ultra-flat bands in twisted bilayer WSe_2. *Nat Commun* 2021; **12**: 5601.

17 Lin Z, Si C, Duan S, *et al.* Rashba splitting in bilayer transition metal dichalcogenides controlled by electronic ferroelectricity. *Phys Rev B* 2019; **100**: 155408.

18 An L, Cai X, Pei D, *et al.* Interaction effects and superconductivity signatures in twisted double-bilayer WSe_2. *Nanoscale Horiz* 2021; **5**: 1309–1316.

19 Resta R. Macroscopic polarization in crystalline dielectrics: The geometric phase approach. *Rev Mod Phys* 1994; **66**: 899–915.

20 Ikeda N, Ohsumi H, Ohwada K, *et al.* Ferroelectricity from iron valence ordering in the charge-frustrated system $LuFe_2O_4$. *Nature* 2005; **436**: 1136–1138.

21 Lunkenheimer P, Müller J, Krohns S, *et al.* Multiferroicity in an organic charge-transfer salt that is suggestive of electric-dipole-driven magnetism. *Nat Mater* 2012; **11**: 755–758.

22 Naik MH, Jain M. Ultraflatbands and shear solitons in moiré patterns of twisted bilayer transition metal dichalcogenides. *Phys Rev Lett* 2018; **121**: 266401.

23 Wang L, Shih EM, Ghiotto A, *et al.* Correlated electronic phases in twisted bilayer transition metal dichalcogenides. *Nat Mater* 2020; **19**: 861–866.

24 Movva HCP, Rai A, Kang S, *et al.* High-mobility holes in dual-gated WSe_2 field-effect transistors. *ACS Nano* 2015; **9**: 10402–10410.

25 Angeli M, MacDonald AH. Γ valley transition metal dichalcogenide moiré bands. *Proc Natl Acad Sci USA* 2021; **118**: e2021826118.

26 Enaldiev VV, Ferreira F, Fal'ko VI. Weak ferroelectric charge transfer in layer-asymmetric bilayers of 2D semiconductors. *Sci Rep* 2021; **11**: 13422.

27 Enaldiev V, Zólyomi V, Yelgel C, *et al.* Stacking domains and dislocation networks in marginally twisted bilayers of transition metal dichalcogenides. *Phys Rev Lett* 2020; **124**: 206101.

28 Qi L, Ruan S, Zeng YJ. Review on recent developments in 2D ferroelectrics: Theories and applications. *Adv Mater* 2021; **33**: 2005098.

29 Cui C, Xue F, Hu WJ, *et al.* Two-dimensional materials with piezoelectric and ferroelectric functionalities. *npj 2D Mater*

Appl 2018; **2**: 18.

30 Guan Z, Hu H, Shen X, *et al.* Recent progress in two-dimensional ferroelectric materials. *Adv Electron Mater* 2020; **6**: 1900818.

31 Magorrian SJ, Enaldiev VV, Zólyomi V, *et al*. Multifaceted moiré superlattice physics in twisted WSe_2 bilayers. *Phys Rev B* 2021; **104**: 125440.

32 Zhang Y, Yuan NFQ, Fu L. Moiré quantum chemistry: Charge transfer in transition metal dichalcogenide superlattices. *Phys Rev B* 2020; **102**: 201115.

33 Li T, Jiang S, Li L, *et al.* Continuous Mott transition in semiconductor moiré superlattices. *Nature* 2021; **597**: 350–354.

34 Liu Y, Zhang J, Meng S, *et al.* Electric field tunable ultrafast interlayer charge transfer in graphene/WS_2 heterostructure. *Nano Lett* 2021; **21**: 4403–4409.

35 Lourtioz JM, Abstreiter G, Meyerson B. *Group IV Heterostructures*, *Physics and Devices* (*Si*, *Ge*, *C*, *Sn*). Oxford: Elsevier Science & Technology, 1998.